
ERROR FEEDBACK CAN ACCURATELY COMPRESS PRECONDITIONERS

Ionut-Vlad Modoranu*

IST Austria

ionut-vlad.modoranu@ist.ac.at

Aleksei Kalinov

IST Austria

aleksei.kalinov@ist.ac.at

Eldar Kurtic

IST Austria

eldar.kurtic@ist.ac.at

Elias Frantar

IST Austria

elias.frantar@ist.ac.at

Dan Alistarh

IST Austria

dan.alistarh@ist.ac.at

ABSTRACT

Leveraging second-order information about the loss at the scale of deep networks is one of the main lines of approach for improving the performance of current optimizers for deep learning. Yet, existing approaches for accurate full-matrix preconditioning, such as Full-Matrix Adagrad (GGT) or Matrix-Free Approximate Curvature (M-FAC) suffer from massive storage costs when applied even to small-scale models, as they must store a sliding window of gradients, whose memory requirements are multiplicative in the model dimension. In this paper, we address this issue via a novel and efficient error-feedback technique that can be applied to compress preconditioners by up to two orders of magnitude in practice, without loss of convergence. Specifically, our approach compresses the gradient information via sparsification or low-rank compression *before* it is fed into the preconditioner, feeding the compression error back into future iterations. Experiments on deep neural networks show that this approach can compress full-matrix preconditioners to up to 99% sparsity without accuracy loss, effectively removing the memory overhead of full-matrix preconditioners such as GGT and M-FAC. Our code is available at <https://github.com/IST-DASLab/EFCP>.

1 Introduction

The remarkable success of stochastic gradient descent (SGD)-based optimizers in deep learning motivated a long line of research for accelerated preconditioned variants that can still scale to the massive parameter and dataset sizes common in the area. Among these, optimizers based on adaptive regularization, such as Adagrad [10] and Adam [18] are extremely well-established, with myriads of extensions, e.g. [2, 1, 38, 14].

Yet, most work in this area restricts preconditioning of the descent direction to a *diagonal matrix*. By contrast, a promising—but considerably less developed—direction employs what we will call *full-matrix preconditioning*, i.e. pre-multiplying the descent direction with a full matrix, whose structure is justified either via adaptive regularization [1], or via approximations of natural gradient such as the Fisher approximation [5, 12].

Yet, existing implementations of full-matrix preconditioning are currently impractical given their massive memory costs. Interestingly, although they have different theoretical justifications, both full-matrix adaptive preconditioning methods such as GGT [1] and full-matrix natural-gradient methods such as M-FAC [12] run into the same key practical limitation: each maintains a “sliding window” of several past gradients, employed in estimating the preconditioner at each step. Even for small-scale models, maintaining the gradient history results in unmanageable total cost of $\Theta(md)$ memory, where d is the model dimension, usually in the millions, and m is the size of the gradient history, usually of size 100-1000. For example, a standard recipe for fine-tuning the medium-scale BERT-base model using the M-FAC preconditioner with standard settings requires more than 450GB of GPU RAM, unavailable on any single GPU. Thus,

*Corresponding author.

while showing promising results in terms of accuracy, full-matrix preconditioning is currently impractical at scale due to memory constraints.

Contribution. In this paper, we present a new algorithmic approach for reducing the massive memory cost of full-matrix preconditioning at the scale of DNNs, called Error Feedback for Compressed Preconditioning (EFCP), which applies to both adaptive (Adagrad/GGT [1]) and natural-gradient (M-FAC [12]) full-matrix preconditioners. In a nutshell, EFCP works by compressing the gradient window either via high sparsity or extremely low rank. In practice, we are able to compress the gradient history by one to two orders of magnitude *without impacting accuracy*, effectively removing the memory limitations of full-matrix preconditioning.

Our results are enabled by two technical innovations. On the conceptual side, the surprising observation behind our work is that the sizable error in the preconditioner induced by gradient sparsification or low-rank projection can in fact be handled via an error feedback mechanism applied to the gradients *before they are stored* into the gradient window. For both variants, we provide efficient compression-aware data structures which can leverage compression for memory savings, and can apply to both M-FAC and GGT.

On the practical side, our main contribution is an efficient GPU implementation for EFCP in the case of high sparsity. Specifically, this is enabled by a novel GPU implementation of a *dynamic sparse ring-buffer* data structure, in which each element is a sparse gradient tensor, and which enables efficient sparse multiplication against new gradients, as needed for preconditioner computations, as well as fast gradient insertions and removals, as required by the sliding window semantics.

We validate our implementation experimentally on standard vision (ResNet/ImageNet) and language modeling (BERT/GLUE) tasks. Results show that EFCP enables us to significantly reduce the memory overhead of full-matrix preconditioning, to the point where it is in the same range as the memory required by standard optimizers such as SGD with Momentum or Adam.

We show this extensively by testing the EFCP implementation in the context of the M-FAC optimizer, compressing gradients to $\sim 99\%$ sparsity (a variant we call Sparse MFAC), as well as via smaller-scale experiments for low-rank compression. Moreover, we show that our implementation is also effective for the GGT full-matrix Adagrad optimizer. For example, for the standard ResNet-18 model [16] *trained from scratch* on ImageNet [30], the Sparse MFAC variant with full-matrix preconditioning uses a maximum of 22.5 GB of GPU RAM, compared to 21.3 GB used by SGD with momentum with the same parameters. At the same time, Sparse MFAC outperforms the well-tuned SGD baseline by approximately 1% Top-1 test accuracy, recovering the accuracy of Dense M-FAC in the same setup (which uses more than 56GB GPU RAM in this setting). We provide additional validation for Sparse M-FAC in the context of training ViT [9] and BERT [8] models as well, and perform ablations w.r.t. sparsity and model size.

In summary, for the first time, EFCP enables experimenting with full-matrix preconditioner methods within the memory capacity of a single GPU in reasonable time, with negligible accuracy loss relative to full preconditioning.

2 Background and Related Work

2.1 General Setting

We consider a standard classification setting, in which we are given a training dataset $\mathcal{D} = \{(x_i, y_i)_{i=1}^N\}$ containing N i.i.d. samples x_i and their associated labels y_i . We suppose input pairs (x, y) are drawn from a true, unknown distribution $p_{true} \triangleq p_t$ having the density $p_t(x, y) = p_t(x)p_t(y|x)$ and our model $\theta \in \mathbb{R}^d$ parameterizes a probabilistic distribution $p_\theta(y|x) \triangleq p(y|f(x, \theta))$ with density $p_\theta(x, y) = p_t(x)p_\theta(y|x)$. Our aim is to minimize the “difference” between the true conditional distribution $p_t(y|x)$ and the modelled conditional distribution $p_\theta(y|x)$, measured in some appropriate metric. If we pick this to be the KL divergence between the two distributions, we obtain the following loss function:

$$KL(p_t(x, y)||p_\theta(x, y)) = \int p_t(x, y) \log \frac{p_t(x, y)}{p_\theta(x, y)} dx dy = \mathbb{E}_{p_t(x)} KL(p_t(y|x)||p_\theta(y|x)) \quad (1)$$

In practice, we only have a finite number of samples $x \sim p_t(x)$ and no information about the density function. In this case, we are using the empirical training distribution \hat{p}_t instead of p_t , which is given by the samples in \mathcal{D} and thus we can define the loss as

$$L(\theta) \triangleq KL(p_t(x, y)||p_\theta(x, y)) = \mathbb{E}_{\hat{p}_t(x)} [KL(p_t(y|x)||p_\theta(y|x))] \approx -\frac{1}{N} \sum_{i=1}^N \log p_\theta(y_i|x_i), \quad (2)$$

which is the standard objective function minimized for the maximum likelihood estimation. The loss $L : \mathbb{R}^d \rightarrow \mathbb{R}$ is assumed to be continuous and twice differentiable.

In practice, the loss $L(\theta)$ defined above is often minimized using variants of Stochastic Gradient Descent (SGD) $\theta_{t+1} \leftarrow \theta_t - \eta_t g_t$, where $g_t \triangleq \nabla_{\theta} L(\theta_t)$ and $\eta_t \in \mathbb{R}$ is the learning rate. However, theoretical results suggest that convergence and end-results can be improved by *preconditioning* this gradient with a matrix C which incorporates information about the geometry of the loss landscape, leading to the parameter update rule

Natural Gradient. A popular approach for estimating a good preconditioner is Natural Gradient [4], which adapts to the information geometry of the loss landscape by measuring the discrepancy between the true distribution and the modelled distribution in terms of KL-divergence in the distribution space, as opposed to using the Euclidean distance as is the case for regular SGD. Then, the preconditioner C is the Fisher Information Matrix (FIM), defined as $F(\theta) \triangleq \frac{1}{N} \sum_{i=1}^N \mathbb{E}_{p_{\theta}(y|x_i)} [\nabla_{\theta} \log p_{\theta}(y|x_i) \nabla_{\theta} \log p_{\theta}(y|x_i)^T]$. In this context, one can show that the FIM is the expected Hessian with respect to the log-likelihood. Since the exact FIM is difficult to compute due to the expectation term in its definition, different efficient approximations of it exist in the literature. For neural networks, K-FAC [13, 25] provides a diagonal and tri-diagonal approximation of FIM by sampling a limited number of y values from $p_{\theta}(y|x_i)$ in order to compute the expectation.

Another popular approximation to the FIM is the Empirical Fisher, defined as $\hat{F}(\theta) \triangleq \frac{1}{N} \sum_{i=1}^N \nabla_{\theta} \log p_{\theta}(y_i|x_i) \nabla_{\theta} \log p_{\theta}(y_i|x_i)^T$. Instead of sample y 's from model's predictive distribution, it uses the associated label y_i . It is important to note that the empirical Fisher is a good approximation of the FIM if $p_t(y|x) \approx p_{\theta}(y|x)$, e.g. when the model has good accuracy. The M-FAC method [12] (Section 2.2) provides an efficient implementation for this approach.

Adaptive Regularization. A different justification for obtaining good preconditioners is via *adaptive regularization*, arising from online convex optimization. Broadly, the idea is to adapt the learning rate corresponding to each parameter in order to minimize regret, defined as the cumulative difference between the optimizer's performance and the best decision in hindsight, by taking into account the history of gradients observed up to a given point. By and large, the community has focused on diagonal preconditioners, which allow computationally-efficient and extremely popular algorithms, such as Adam [18] and AdaGrad [10]. The GGT result [1] (Section 2.2) showed that results can be improved by taking "second-order" weight correlations into account, leading to a full-matrix, $d \times d$ preconditioner, and provided an efficient approximation of this preconditioner.

2.2 Efficient Full-Matrix Preconditioners

Overview. We now provide a detailed description of the M-FAC full-matrix preconditioner [12], which will serve as the main illustration of our preconditioner compression method in the paper body. A fully-worked-out example for the GGT preconditioner [1] is also provided in the Appendix. A common point of both methods is that they store a history of the past m gradients in the matrix

$$G = [g_{t-(m-1)}^T, g_{t-(m-2)}^T, \dots, g_{t-1}^T, g_t^T] \in \mathbb{R}^{m \times d}, \quad (3)$$

which can be represented as a ring buffer, updated at each step by replacing the oldest gradient $g_{t-(m-1)}$ with the most recently-generated one g_t . (The main difference between M-FAC and GGT comes from the way the ring buffer G is used to approximate the preconditioner.) To preserve performance, the buffer G_t must be stored in the GPU memory. For best accuracy, both methods require storing a large window of m gradients, where m is usually between 100 and 1000, each of which are of size d (the model dimension). Thus, the memory cost of each method becomes intractable in large-scale settings. Next, we briefly describe the algorithmic implementation of M-FAC.

The M-FAC Optimizer. M-FAC provides an efficient estimator for Inverse-Hessian-Vector-Products (IHVPs) for the special case where the Hessian is approximated via the Empirical Fisher approximation $\hat{F} = \frac{1}{m} \sum_{i=1}^m g_i g_i^T$, where the gradients $g_t \triangleq \nabla_{\theta} L(\theta_t)$ are stored in the matrix G , defined above. The first idea is to use the classic Woodbury-Sherman-Morrison (WSM) formula to integrate new gradient information as rank-1 updates into the current inverse. This leads to the following recursion to compute the IVHPs with an arbitrary vector $x \in \mathbb{R}^d$ as

$$\hat{F}_{t+1}^{-1} x = \left(\hat{F}_t + \frac{1}{m} g_t g_t^T \right)^{-1} x \stackrel{\text{WSM}}{=} \hat{F}_t^{-1} x - \frac{\hat{F}_t^{-1} g_t (\hat{F}_t^{-1} g_t)^T}{m + g_t^T \hat{F}_t^{-1} g_t} x = \frac{1}{\lambda} x - \sum_{k=1}^t \frac{\hat{F}_k^{-1} g_k (\hat{F}_k^{-1} g_k^T)}{m + g_k^T \hat{F}_k^{-1} g_k} x, \quad (4)$$

where $F_0 = \lambda I_d$ and $\lambda > 0$ is a damping parameter.

The key technical idea behind M-FAC is the authors' non-trivial observation that IHVPs can be expressed as a linear combination between the past gradients in the sliding window, where the coefficients are efficiently computed based only on scalar products $g_i^T g_j$ and $g_i^T x$, leading to the following expression for the IHVPs as

$$\hat{F}_m^{-1} x = \frac{1}{\lambda} x - \sum_{k=1}^m c_k g_k. \quad (5)$$

This allows M-FAC to efficiently add or remove gradients from the sliding window, done by computing the corresponding coefficients c_k , and then making the resulting update into the formula for $\hat{F}_m^{-1}x$.

A key aspect regarding M-FAC is the interaction with regularization. Recent work [40] explains that weight decay and L_2 -regularization coincide for SGD, but are different for preconditioned methods. Simply inputting $g_t = \nabla_{\theta}L(\theta) + \gamma\theta$ into the M-FAC preconditioner invalidates the empirical Fisher definition due to the additional term $\gamma\theta$. Based on this, and differing from M-FAC [12], we will decouple the regularization such that the empirical Fisher definition holds and use the update $\theta_{t+1} = (1 - \gamma\eta_t)\theta_t - \eta_t\hat{F}_t^{-1}\nabla_{\theta}L(\theta_t)$, where $\gamma > 0$ is the weight decay parameter.

Data Structures and Operations. Next, we briefly summarize the main operations in the original M-FAC optimizer (denoted next by Dense M-FAC). We detail the challenges that appear when the internal buffer G is sparse, as well as our GPU-efficient solution, in the further sections. First, notice that the main operations in M-FAC are the Scalar Products (SP) and the Linear Combination of Gradients (LCG), which are needed to express the IHVPs as a linear combination.

Scalar Products (SP). This first operation corresponds to the pairwise scalar products of rows in $G \in \mathbb{R}^{m \times d}$ stored in an intermediary matrix $S = GG^T \in \mathbb{R}^{m \times m}$, where $S_{ij} = g_i^T g_j$. When the buffer G is updated (e.g. the oldest gradient is replaced by a new gradient $g \in \mathbb{R}^d$ at row i), the i^{th} row and i^{th} column of matrix S are updated as $S_{:,i} = S_{:,i} + G \cdot g \in \mathbb{R}^m$. This operation can be easily performed on GPU using frameworks such as Pytorch.

Linear Combination of Gradients (LCG). The second main operation of M-FAC is the linear combination of gradients, having the coefficients vector $c \in \mathbb{R}^m$. For a *dense* buffer G , the LCG is easily computed by multiplying each component c_i with the i^{th} row of G and then computing the sum of all rows in G . This operation can also be easily performed in PyTorch on GPU.

2.3 Related Methods

In the Appendix, we provide a full discussion of GGT [1], as well as its compressed version, which can be seen as a full-matrix version of AdaGrad optimizer. More generally, obtaining efficient approximations of second-order (curvature) information in deep learning is an active area. The *diagonal* approximation of the Hessian [19, 18] is very popular; however, it is known to provide lower quality relative to both block-wise methods or K-FAC [37, 32, 12].

K-FAC provides a block diagonal approximation of the FIM, and allows efficient computation of the inverse [6, 29, 39, 37, 21]; however, it is known that its prerequisites do not always hold [26]. *Hessian-free* optimization [24] forgoes the explicit computation of Hessians in favor of computing an IHVP, but may require several “inner” iterations to converge at each step. AdaHessian [38] provided an alternative approximation of the inverse Hessian diagonal, using Hutchinson’s randomized algorithm for estimating the diagonal, which requires smoothing heuristics, and has at least 2x theoretical iteration cost vs SGD, which in practice is usually around 3x. Shampoo [14] provides an efficient heuristic approximation of GGT, reducing memory cost by maintaining preconditioner estimates per model tensor, using an efficient iterative method to compute preconditioner inverses.

The Error Feedback Mechanism. The error feedback mechanism has been studied extensively in the context of gradient compression for standard SGD, in the absence of complex preconditioning. The first analyses of sparsified SGD with error feedback were provided by [33, 3] under additional assumptions, while [17, 34, 27] provided additions to the analysis. More recently, a very complex argument by [23] analyzed convergence of diagonal Adagrad with error feedback. We show that their analysis extends to a diagonal version of our algorithm.

3 Method

Algorithm 1 EFPCP: Error Feedback for Accurate Compressed Full-Matrix Preconditioning

```

1: Parameters:  $T$  = steps count;  $m$  = gradient count;
2:  $\xi_0 = 0_d \in \mathbb{R}^d$  ▷ initialize error feedback
3: for each step  $t \in \{1, 2, \dots, T\}$  do
4:    $g_t \leftarrow \nabla_{\theta}L(\theta_t)$  ▷ get gradient
5:    $a_t \leftarrow \xi_{t-1} + g_t$  ▷ error feedback
6:    $c_t \leftarrow \text{COMPRESS}(a_t)$  ▷ compress the accumulator
7:    $\xi_t \leftarrow a_t - c_t$  ▷ update the error
8:    $u_t \leftarrow \mathcal{A}(c_t)$  ▷ update  $G$  and precondition using  $\mathcal{A}$ 
9:    $\theta_t \leftarrow \theta_{t-1} - \eta_t u_t$  ▷ update model parameters
10: end for

```

Overview. Our general approach for compressing the gradient history required by full-matrix preconditioners is described in Algorithm 1. Conceptually, we assume a standard gradient-based optimization setup with an oracle g_t at each step t , augmented by a preconditioning algorithm \mathcal{A} , based on a gradient sliding window G , whose large memory cost we want to reduce. We propose to do this by feeding *compressed* gradients into the preconditioner estimate maintained by algorithm \mathcal{A} . Yet, doing so directly by projecting the gradients onto a sparse or low-rank support diverges.

Instead, we apply *error feedback* [31, 3, 17] to gradients *before they are fed into the preconditioner data structure*, using an error accumulator vector $\xi_t \in \mathbb{R}^d$, initially set to zero. At each step, we obtain the gradient g_t of the model parameters w.r.t. the loss, after which we feed back the error ξ_{t-1} into the current gradient g_t , obtaining the *accumulator* a_t . Next, the accumulator a_t is compressed, using e.g. sparsity or low-rank, to obtain a compressed representation c_t . The compression error ξ_t is updated to the difference between the accumulator a_t and its compressed version c_t . Finally, the compressed gradient c_t is fed directly to the preconditioning algorithm \mathcal{A} .

Notice that, other than the three lines corresponding to error feedback (blue in the algorithm), the optimization loop is the same as the uncompressed one. However, we emphasize that the internal buffer of the preconditioned optimizer will store a sequence of m representations $[c_{t-(m-1)}, c_{t-(m-2)}, \dots, c_{t-1}, c_t]$, each of which is highly-compressed, leading to memory savings.

While this blueprint appears simple, two key questions remain: (1) *how can we leverage the compressed gradient window for actual memory and computational speedups on complex real-world preconditioners?* and (2) *why does this approach preserve convergence?* We address them below.

3.1 Compressing Preconditioners via Sparsity

We now expand on accumulator compression via sparsity, specifically by using Top- k sparsification and error feedback. Specifically, the preconditioner data structure will only store $k \ll d$ entries from each accumulated gradient, where k is around 1% of the full dimension d . As we will show experimentally, this will essentially remove the memory overhead of full-matrix preconditioning.

We detail our approach for the Sparse M-FAC algorithm; the Sparse GGT variant is slightly simpler and is described in Appendix D due to space limitations. For Sparse M-FAC, we describe the changes required by sparsity for the buffer G and the Scalar Product (SP) and Linear Combination of Gradients (LCG) operations. A key concern will be re-interpreting the mathematical formulation in order to be able to leverage fast CUDA kernels, which is notoriously challenging in the context of sparsity.

Sparsity format for G . To store the gradient history G , we need a sparse matrix-like data structure for storing gradients that fulfills the following two properties at the same time: i) it allows easy replacement of any row (corresponding to adding and removing gradients) and ii) it allows computing the scalar product (SP) and linear combination of gradients (LCG) operations efficiently. To the best of our knowledge, no such data structure is known in the literature.

Specifically, for Sparse M-FAC, we want to input sparse accumulators c_t of size $k \ll d$ into the buffer G . Instead of storing $G \in \mathbb{R}^{m \times d}$ densely, we will store $G = (\mathcal{I}, \mathcal{V})$, where $\mathcal{I} \in \mathbb{N}^{m \times k}$ will store the indices returned by Top- k and $\mathcal{V} \in \mathbb{R}^{m \times k}$ will store the corresponding values. When the j^{th} row of G is updated with the new indices-values pair (i_j, v_j) , we replace the j^{th} row in \mathcal{I} and \mathcal{V} with i_j and v_j , respectively. Breaking G into two matrices of indices and values means that G loses the matrix structure in the dense sense and the SP and LCG operations must be redefined because we cannot use the basic PyTorch operations for matrix multiplications anymore. Below we describe our solution for these two operations that involve CUDA specific kernels to efficiently perform the computations on a GPU for large models, but first we would like to provide details about the sparsity pattern which we can leverage to obtain more efficient kernels for our particular problem.

Sparsity Pattern. One observation is that, due to the algorithm structure, each row in $G = (\mathcal{I}, \mathcal{V})$ has the same sparsity. To leverage this, at each step we compress the accumulator a_t using Top- k applied in blocks of (large) fixed size B . We do this to have selected values uniformly chosen in order to speed up the LCG operation (details below). We express k as a percentage of total number of weights d and then convert it to a particular integer value that represents the density of values used in the Top- k call. For example, in most of our experiments we will have $k = 1\%$, meaning that for each block of size B we will have roughly $B/100$ non-zero values. This way we know that for any block of size B we have the same number of weights in a specific interval. We provide more details about choosing B in the section where we describe the LCG operation.

Format for \mathcal{V} . Starting with the CUDA capability 8.0, the Nvidia GPUs have bfloat16 support, which is a half precision data type optimized for Deep Learning. We found that our optimizer still converges when we use bfloat16 instead of

float32. This is particularly useful when automatic mixed precision (AMP) is activated because it speeds up the overall training and has a lower memory footprint (both for the model’s state and for the optimizer’s state).

Sparse Scalar Products. This operation is commonly known as sparse-matrix vector multiplication (SPMV) and several implementations already exist for a few sparsity representations (e.g. CSR, COO), but unfortunately they cannot be directly used for our particular choice for the matrix $G = (\mathcal{I}, \mathcal{V})$, each of size $m \times k$. Thus, we can write a kernel that leverages the properties of our buffer as follows. We use m thread blocks, each containing 1024 threads. One thread block processes one row and has a shared memory array of 1024 floats to store the dot product computed on a subset of the row. We perform memory coalesced reads for the indices and values from the global memory. In the end, we perform parallel reduction over the shared memory buffer to compute the sum (the final value for the dot product) in logarithmic complexity. We show our implementation of the SP operation in the Appendix C.

Sparse LCG. This operation leverages the block sparsity to efficiently compute the linear combination of gradients. Given that we apply sparsity in blocks of size B , we know that in every block we will always have a fixed number of values (and indices) selected by Top- k (e.g., for $B = 10000$ and $k = 1\%$, we will have 100 values and indices in any interval $[n \cdot B, (n + 1) \cdot B] \cap \mathbb{N}$, with $n \in \mathbb{N}$). This allows us to use a shared memory block to accumulate the linear combination of gradients across a slice of size $m \times B$ from $G = (\mathcal{I}, \mathcal{V})$ and write the content of the shared memory at the correct offsets in the global memory that stores the result (here, we use the information that the indices are in a specific interval). Similar to the SP case, we also perform memory coalesced reads for the indices and values from the global memory only once for each component. We provide explanations about how we choose the thread blocks dimensions in the next paragraph and we show our implementation of the LCG operation in the Appendix C.

Thread Blocks for LCG. Choosing the right number of thread blocks is critical for the performance of the Sparse LCG, since it needs to balance memory transfer and compute load. To address this, we provide an automatic procedure for choosing this parameter, based on the GPU capabilities. Specifically, given a number of threads and maximum available GPU shared memory size, we determine the total number of thread blocks to be used to allow for full utilization, avoiding waiting in the queue at each SM.

Efficiency Improvements. These technical data structure optimizations are critical for good performance. Relative to a naive Pytorch implementation of the same approach, which stores the gradients as sparse but performs the operations in dense format, the above approach is 1.5-2x faster and uses 20-30% less memory.

Memory Savings. Compressing the buffer using sparsity yields $\tilde{O}(mk)$ space complexity, where k is the target density of the gradients after Top- k compression, ignoring logarithmic factors due to indexing. In practice, we obtain stable convergence for $k = d/100$, which translates into practical space savings of approximately 20x (relative to GGT) and 30x (relative to M-FAC). We provide exact numbers in the experimental section.

3.2 Low-Rank Compression of Preconditioners

In Appendix E, we discuss low-rank compression of the gradients used in the preconditioner. Specifically, this requires re-implementing the COMPRESS step in Algorithm 1 via a low-rank approximation of the gradient, which we do using an efficient variant of power iteration [35]. Then, we again consider the M-FAC algorithm and reformulate its algebraic operations to leverage low-rank matrices for memory and computational savings.

4 Experiments

We now validate our results experimentally. In the main text, we focus on comparing Sparse M-FAC with other optimizers, as it proved to be the most practical variant of EFCP. We show results for low-rank M-FAC and Sparse GGT in the Appendix.

In the following, we validate Sparse MFAC (S-MFAC) experimentally as an optimizer for training in the context of standard vision and language modelling tasks. Specifically, we integrate our S-MFAC optimizer in ASDL [28], a benchmarking library for second-order optimizers, but also examine larger-scale tasks such as ImageNet training of ResNet-18 and compare S-MFAC with AdamW and Dense M-FAC (D-MFAC) on BERT models on GLUE tasks. We report training loss, test accuracy and total running times and top memory usage for the entire training process.

Notations. We use the notation E for number of epochs, η for learning rate, γ for weight decay, B for batch size, m for the number of gradients (sliding window size), $k = 1\%$ the gradient density. We use the prefixes **D** for **D**ense and **S** for **S**parse in the context of adaptive optimizers M-FAC. For the gradient window size m , we use the standard settings for D-MFAC [12], which is $m = 1000$ unless otherwise specified.

The ASDL Benchmark. In the first experiment, we integrate S-MFAC into the ASDL benchmarking framework for second-order optimizers [28], for the task of fine-tuning a ViT-T model pre-trained on ImageNet. We report the test

accuracy for the run that has largest validation accuracy. Table 1 shows the test accuracy of our S-MFAC optimizer compared to the other optimizers reported in the paper. (We had to remove P-SGD from the comparison due to errors raised by the implementation during experiments.) We observe that S-MFAC is competitive with other preconditioned gradient methods, outperforming SGD, AdamW, K-FAC and SENG, and matching the highest accuracy obtained on this task (98%) with affordable time and memory overheads relative to SGD.

Table 1: Test accuracy of S-MFAC for ResNet-18 and ViT-Tiny on CIFAR-10. The accuracies for the other optimizers are obtained from ASDL [28]. We also report relative time and memory overheads w.r.t. SGD.

Optimizer	ViT-T	Time	Memory
SGD	97.8	1×	1×
AdamW	97.9	1×	1.01×
K-FAC(1mc)	97.4	1.12×	1.13×
SENG	97.7	35×	7.31×
Shampoo	98.0	1.6×	1.07×
S-MFAC	98.0	1.63×	1.15×

ImageNet/ResNet-18. Next, we move to a more complex vision task, by training ResNet-18 on ImageNet [7] *from scratch* using a highly-tuned version of SGD (with momentum) from the FFCV [22] library, as well as S/D-MFAC. All hyper-parameters are provided in the Appendix A. Figure 1 shows the validation accuracy curves for this experiment, while Figure 2 shows the best achieved training loss and validation accuracy for each method, including a detailed sparsity sweep below 1% density for S-MFAC. (The loss curves show similar trends, and are provided in the Appendix.)

We begin by noting that SGD obtains training loss 2.237 with accuracy 69.12%. D-MFAC reaches 2.164 loss and significantly higher Top-1 validation accuracy, 70.03%. Despite slightly higher training loss than D-MFAC (2.185), S-MFAC has comparable 70.01% validation accuracy, which is very strong for this model and training recipe. Thus, even for this challenging task, compressing the preconditioner essentially recovers the accuracy of the dense M-FAC optimizer. When we examine the behavior of S-MFAC as we decrease gradient density, we observe that, remarkably, S-MFAC with $k = 0.17\%$ (only $\approx 20k$ entries!) still achieves comparable accuracy to SGD, and that accuracy decreases gradually. However, the resulting preconditioned gradients are not necessarily very sparse.

To examine memory, we ran the experiments on a single A100 GPU and recorded the max memory usage throughout the entire process via the NVIDIA-SMI tool. We find that SGD uses 12.8 GB and S-MFAC 14.3 GB, while D-MFAC in the same setting needs 59 GB.

BERT/GLUE-MNLI. Finally, we test our S-MFAC implementation for BERT-TINY/MINI/BASE models on the MNLI task from the GLUE benchmark [36], comparing against the Adam optimizer with optimized default settings from Hugging Face [8], which reproduce or improve upon the original paper [8]. Dense M-FAC with a window size of $m = 1024$ can only be executed on the TINY and MINI model variants, requiring 18 GB and 45 GB memory, respectively, and runs out of memory (OOM) for the BASE model (the required memory usage for the ring buffer G alone is 417GB).

The results in Table 2 show that our S-MFAC implementation not only recovers the performance of D-MFAC on BERT-TINY/MINI, but also allows us to run on BERT-base, with superior validation accuracy relative to Adam using standard hyper-parameters (e.g., learning rate $\eta = 2e - 5$). For the TINY model S-MFAC achieves almost 2% higher accuracy compared to D-MFAC and close to 5% higher validation accuracy compared to Adam. The former improvement can be justified by the regularization effect of sparsity relative to D-MFAC, as this is a fine-tuning task, whereas the latter is due to leveraging second-order information.

At the same time we observe that, accuracy differences become smaller as model size increases. This behavior is also reported in the original D-MFAC [12] optimizer for the same GLUE/MNLI task. While this is another indication that the sparse implementation preserves the behavior of the dense counterpart, it suggests that the benefits of second-order information diminish in the case of over-parametrized fine-tuning tasks.

Table 2: Evaluation accuracy for BERT-Tiny/Mini/Base on GLUE-MNLI. OOM stands for Out of Memory error.

	T	M	B
Adam	66.86	74.77	84.6
S-MFAC	71.06	76.40	84.86
D-MFAC	69.26	76.39	OOM

Figure 1: Validation (Top-1) accuracy for ResNet18 training from scratch on ImageNet-1K. M-FAC and 99%-Sparse M-FAC reach approximately 1% higher validation accuracy relative to SGD using the well-tuned FFCV recipe [22].

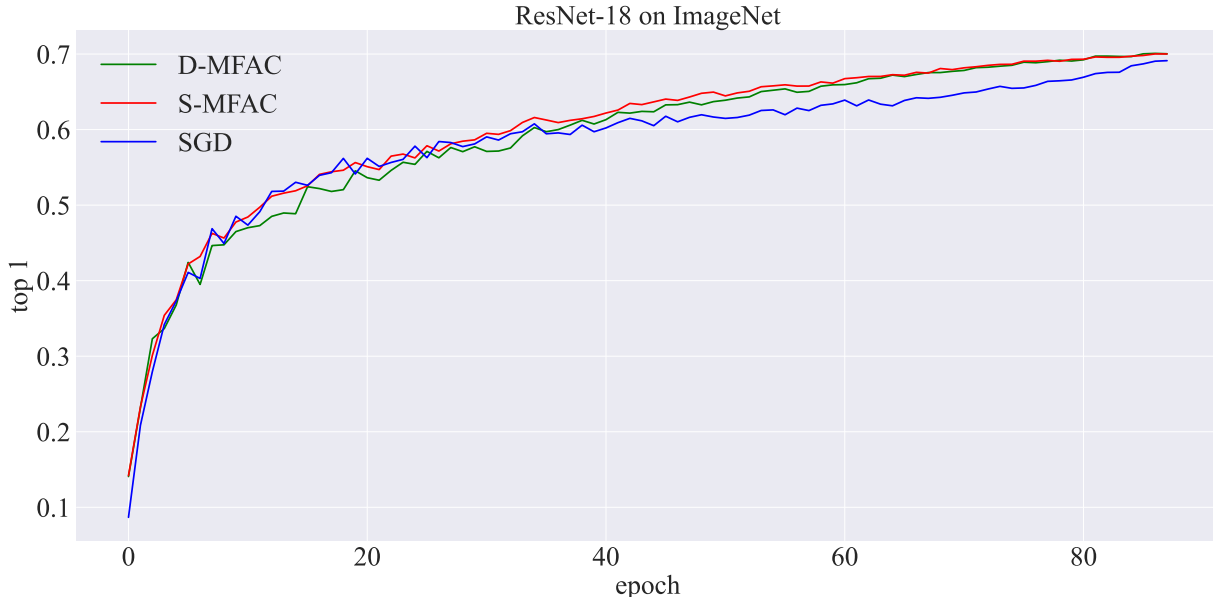


Figure 2: Training loss and validation (Top-1) accuracy for ResNet18 training from scratch on ImageNet-1K under a detailed sparsity sweep, between 1% and 0.04% density. Dense M-FAC outperforms SGD in this setting by about 1%, which is recovered by S-MFAC at 1% density. Even with 0.17% gradient density, M-FAC slightly outperforms SGD in terms of training loss and test accuracy.

Density k	Train Loss	Test Accuracy
D-MFAC (100%)	2.164	70.03%
117k (1.00%)	2.185	70.01%
100k (0.85%)	2.183	70.18%
75k (0.64%)	2.187	69.99%
50k (0.42%)	2.190	69.68%
25k (0.21%)	2.206	69.43%
20k (0.17%)	2.217	69.26%
15k (0.12%)	2.230	69.05%
10k (0.08%)	2.246	68.84%
5k (0.04%)	2.300	68.27%
SGD	2.237	69.12%

Running times and memory usage. Finally, we examine running times and memory usage for the algorithm. The results across our experiments are shown in Table 3. We note that, in the current implementation, both D-MFAC and our optimizer have a constant additional cost relative to the highly-optimized Adam or SGD implementations in Pytorch, due to the additional data structures employed. This cost can be reduced via optimizations.

Specifically, our current implementation was primarily optimized for residual networks. This is reflected in the runtime and memory numbers: on ResNet-18 (11.7M params), D-MFAC requires $4.6\times$ more memory compared to SGD with momentum and 25% larger running time. Our S-MFAC implementation diminishes these costs, bringing both the running time and memory usage to be almost negligible compared to SGD. Specifically, the memory usage is 25% of D-MFAC.

For BERT-TINY (4M params), D-MFAC uses $14\times$ more memory and BERT-MINI (11M params) uses $15\times$ more memory compared to S-MFAC. Further, we find that EFCP is extremely effective for large models like BERT-BASE (110M params). In this case, running D-MFAC would raise an out of memory (OOM) error (just the dense ring buffer used to store the gradient window requires 417 GB of memory under standard parameters).

Table 3: Running times and memory usages for ImageNet/ResNet-18 and GLUE/BERT reported on an NVIDIA A100 GPU with 82GB RAM. OOM stands for Out Of Memory.

Model	Optimizer	Memory	Training Time
ResNet-18	SGD	12.8 GB	4h 10m
	S-MFAC	14.3 GB	4h 21m
	D-MFAC	58.5 GB	5h 33m
BERT-Tiny	Adam	0.8 GB	11m
	S-MFAC	1.3 GB	1h 5m
	D-MFAC	17.9 GB	1h 20m
BERT-Mini	Adam	1.3 GB	21m
	S-MFAC	2.9 GB	1h 5m
	D-MFAC	44.9 GB	1h 50m
BERT-Base	Adam	7.1 GB	1h 45m
	S-MFAC	14.8 GB	3h 20m
	D-MFAC	OOM	-

Although our primary concern in experiments is memory cost, we observe that, in terms of running time, our algorithm has essentially no overhead on ResNet-18. On BERT models, there is a notable runtime overhead, which is due in part to the fact that our CUDA kernels are not specifically adapted to BERT models. We expect this overhead to be reduced via tuning and further optimizations, which we plan to investigate in future work. However, we note that these single-GPU runtimes are very manageable already.

To decrease memory usage and running time, one can try reducing the number of gradients m . However, it is clear from prior work [1, 12] that large values of m are needed to provide better accuracy results, and specifically to improve over standard baseline. This is theoretically motivated in part by the fact that the rank of matrix G is at most m , which can be extremely low compared to the rank of Hessian matrix for large models and the approximation would be very poor for low values of m . Thus, large models require large number of gradients m , which renders our technique effective. To our knowledge, our approach allows full-matrix adaptive optimizers to be run on a consumer GPU for the first time. Appendix B contains a detailed theoretical analysis for memory savings.

5 Conclusions and future work

We have provided a versatile new tool for addressing the memory costs of adaptive full-matrix preconditioning, in the form of a series of methods which compress the gradient history, by leveraging an instance of the error feedback mechanism. We complement this mechanism via efficient sparse/low-rank algorithms for maintaining existing preconditioners, and have shown experimentally that our approach can essentially provide lossless compression when applied via sparsity, with remarkably large compression rates. We provide CUDA implementations for a sparse data structure that 1) allows easy replacement of any row (adding/replacing new compressed representations of error feedback accumulators and 2) allows computing the SP and LCG operations efficiently which, to the best of our knowledge, is the first such data structure known in the literature.

In future work, we plan to further investigate theoretical justification for our method. Obtaining general bounds appears extremely challenging, as even in the case of standard SGD understanding error feedback required significant technical effort, e.g. [3, 17]. Another direction of future work is exploring larger-scale validation of our method for additional architectures and tasks, and for additional preconditioning mechanisms.

Acknowledgements

The authors thank Adrian Vladu, Alexandra Peste, Mher Safaryan and Elias Frantar for their valuable feedback, the IT department from Institute of Science and Technology Austria for the hardware support and Weights and Biases for the infrastructure to track all our experiments.

References

- [1] Naman Agarwal, Brian Bullins, Xinyi Chen, Elad Hazan, Karan Singh, Cyril Zhang, and Yi Zhang. Efficient full-matrix adaptive regularization. In *International Conference on Machine Learning*, pages 102–110. PMLR,

- 2019.
- [2] Naman Agarwal, Brian Bullins, and Elad Hazan. Second-order stochastic optimization for machine learning in linear time, 2016.
 - [3] Dan Alistarh, Torsten Hoefler, Mikael Johansson, Nikola Konstantinov, Sarit Khirirat, and Cédric Renggli. The convergence of sparsified gradient methods. In *Advances in Neural Information Processing Systems*, pages 5973–5983, 2018.
 - [4] S.-I. Amari. Natural gradient works efficiently in learning, 1998.
 - [5] Shun-ichi Amari. Natural gradient works efficiently in learning. *Neural Computation*, 10(2):251–276, 1998.
 - [6] Jimmy Ba, Roger Grosse, and James Martens. Distributed second-order optimization using kronecker-factored approximations. <https://openreview.net/forum?id=SkkTMPjex>, 2016.
 - [7] Jia Deng, Wei Dong, Richard Socher, Li-Jia Li, Kai Li, and Li Fei-Fei. Imagenet: A large-scale hierarchical image database. In *2009 IEEE conference on computer vision and pattern recognition*, pages 248–255. Ieee, 2009.
 - [8] Jacob Devlin, Ming-Wei Chang, Kenton Lee, and Kristina Toutanova. Bert: Pre-training of deep bidirectional transformers for language understanding, 2018.
 - [9] Alexey Dosovitskiy, Lucas Beyer, Alexander Kolesnikov, Dirk Weissenborn, Xiaohua Zhai, Thomas Unterthiner, Mostafa Dehghani, Matthias Minderer, Georg Heigold, Sylvain Gelly, et al. An image is worth 16x16 words: Transformers for image recognition at scale. In *Proceedings of the Ninth International Conference on Learning Representations*, 2021.
 - [10] John C. Duchi, Elad Hazan, and Yoram Singer. Adaptive subgradient methods for online learning and stochastic optimization. *J. Mach. Learn. Res.*, 12:2121–2159, 2010.
 - [11] Matthias Fey et al. Pytorch-sparse library. https://github.com/rusty1s/pytorch_sparse.
 - [12] Elias Frantar, Eldar Kurtic, and Dan Alistarh. M-fac: Efficient matrix-free approximations of second-order information, 2021.
 - [13] Roger Grosse and James Martens. A kronecker-factored approximate fisher matrix for convolution layers, 2016.
 - [14] Vineet Gupta, Tomer Koren, and Yoram Singer. Shampoo: Preconditioned stochastic tensor optimization. In *International Conference on Machine Learning*, pages 1842–1850. PMLR, 2018.
 - [15] Kaiming He, Xiangyu Zhang, Shaoqing Ren, and Jian Sun. Deep residual learning for image recognition, 2015.
 - [16] Kaiming He, Xiangyu Zhang, Shaoqing Ren, and Jian Sun. Deep residual learning for image recognition. *2016 IEEE Conference on Computer Vision and Pattern Recognition (CVPR)*, Jun 2016.
 - [17] Sai Praneeth Karimireddy, Quentin Rebjock, Sebastian U Stich, and Martin Jaggi. Error feedback fixes SignSGD and other gradient compression schemes. In *Proceedings of the Thirty-sixth International Conference on Machine Learning*, pages 3252–3261, 2019.
 - [18] Diederik P. Kingma and Jimmy Ba. Adam: A method for stochastic optimization, 2014.
 - [19] Shankar Krishnan, Ying Xiao, and Rif A Saurous. Neumann optimizer: A practical optimization algorithm for deep neural networks. *arXiv preprint arXiv:1712.03298*, 2017.
 - [20] Alex Krizhevsky, Vinod Nair, and Geoffrey Hinton. Cifar-10 (canadian institute for advanced research). <https://www.cs.toronto.edu/~kriz/cifar.html>, 2009.
 - [21] César Laurent, Thomas George, Xavier Bouthillier, Nicolas Ballas, and Pascal Vincent. An evaluation of fisher approximations beyond kronecker factorization, 2018.
 - [22] Guillaume Leclerc, Andrew Ilyas, Logan Engstrom, Sung Min Park, Hadi Salman, and Aleksander Madry. FFCV: Accelerating training by removing data bottlenecks. <https://github.com/libffcv/ffcv/>, 2022.
 - [23] Xiaoyun Li, Belhal Karimi, and Ping Li. On distributed adaptive optimization with gradient compression. *arXiv preprint arXiv:2205.05632*, 2022.
 - [24] James Martens. Deep learning via hessian-free optimization. In *Proceedings of the 27th International Conference on International Conference on Machine Learning*, ICML’10, page 735–742, Madison, WI, USA, 2010. Omnipress.
 - [25] James Martens, Jimmy Ba, and Matt Johnson. Kronecker-factored curvature approximations for recurrent neural networks. In *International Conference on Learning Representations*, 2018.
 - [26] James Martens and Roger Grosse. Optimizing neural networks with kronecker-factored approximate curvature, 2015.

- [27] Giorgi Nadiradze, Iliia Markov, Bapi Chatterjee, Vyacheslav Kungurtsev, and Dan Alistarh. Elastic consistency: A general consistency model for distributed stochastic gradient descent. *arXiv preprint arXiv:2001.05918*, 2020.
- [28] Kazuki Osawa, Satoki Ishikawa, Rio Yokota, Shigang Li, and Torsten Hoefer. Asdl: A unified interface for gradient preconditioning in pytorch, 2023.
- [29] Kazuki Osawa, Yohei Tsuji, Yuichiro Ueno, Akira Naruse, Rio Yokota, and Satoshi Matsuoka. Large-scale distributed second-order optimization using kronecker-factored approximate curvature for deep convolutional neural networks. *2019 IEEE/CVF Conference on Computer Vision and Pattern Recognition (CVPR)*, Jun 2019.
- [30] Olga Russakovsky, Jia Deng, Hao Su, Jonathan Krause, Sanjeev Satheesh, Sean Ma, Zhiheng Huang, Andrej Karpathy, Aditya Khosla, Michael Bernstein, et al. Imagenet large scale visual recognition challenge. *International Journal of Computer Vision*, 115(3):211–252, 2015.
- [31] Frank Seide, Hao Fu, Jasha Droppo, Gang Li, and Dong Yu. 1-bit stochastic gradient descent and its application to data-parallel distributed training of speech DNNs. In *Fifteenth Annual Conference of the International Speech Communication Association*, 2014.
- [32] Sidak Pal Singh and Dan Alistarh. Woodfisher: Efficient second-order approximation for neural network compression, 2020.
- [33] Sebastian U Stich, Jean-Baptiste Cordonnier, and Martin Jaggi. Sparsified sgd with memory. *Advances in Neural Information Processing Systems*, 31, 2018.
- [34] Sebastian U Stich and Sai Praneeth Karimireddy. The error-feedback framework: Better rates for sgd with delayed gradients and compressed communication. *arXiv preprint arXiv:1909.05350*, 2019.
- [35] Thijs Vogels, Sai Praneeth Karimireddy, and Martin Jaggi. PowerSGD: Practical Low-Rank Gradient Compression for Distributed Optimization. In *Advances in Neural Information Processing Systems*, volume 32. Curran Associates, Inc., 2019.
- [36] Alex Wang, Amanpreet Singh, Julian Michael, Felix Hill, Omer Levy, and Samuel R Bowman. GLUE: A multi-task benchmark and analysis platform for natural language understanding. In *Proceedings of the Seventh International Conference on Learning Representations*, 2019.
- [37] Chaoqi Wang, Roger Grosse, Sanja Fidler, and Guodong Zhang. Eigendamage: Structured pruning in the kronecker-factored eigenbasis, 2019.
- [38] Zhewei Yao, Amir Gholami, Sheng Shen, Kurt Keutzer, and Michael W Mahoney. Adahessian: An adaptive second order optimizer for machine learning. *arXiv preprint arXiv:2006.00719*, 2020.
- [39] Wenyuan Zeng and Raquel Urtasun. MLPrune: Multi-layer pruning for automated neural network compression, 2019.
- [40] Guodong Zhang, Chaoqi Wang, Bowen Xu, and Roger Grosse. Three mechanisms of weight decay regularization, 2018.

Appendices

A Hyper-parameters

We restate the notations that we introduced in the main body of our work. We use notation μ for momentum, η for the initial learning rate, γ for weight decay, λ for M-FAC dampening, k for gradient density, ρ for rank, E for epochs, B for batch size.

A.1 ASDL

We perform hyper-parameter tuning for CIFAR-10 and ViT-Tiny, as described in the appendix section of the ASDL [28] paper. Concretely, the general grids we use are $\{32, 128, 512, 2048\}$ for the batch size, $\{3e-1, 1e-1, 3e-2, 1e-2, 3e-3, 1e-3\}$ for the learning rate, $E = 20$ epochs, we clip the preconditioned gradient norm to 10 and perform grid search for the dampening parameter λ over the grid $\{1e-2, 5e-3, 1e-3, 5e-4, 1e-4, 5e-5, 1e-5, 5e-6, 1e-6\}$ for S-MFAC. In particular, ViT-Tiny uses $\gamma = 1e-4$.

A.2 FFCV

For the ImageNet dataset and ResNet-18 model, we use $E = 88$ epochs, batch size $B = 1024$, linear decay schedule for the learning rate η . In particular, we set the weight decay $\gamma = 1e-5$ for convolution and fully connected parameters and $\gamma = 0$ for batch-normalization parameters, thus fixing the issue in the main FFCV repository. We use linear learning rate decay for all three optimizers and disable image rescaling. We present the final hyper-parameters in Table 6.

A.3 BERT/GLUE

We use the HuggingFace repository and plug in our D/S-MFAC optimizers. We compare against default Adam baselines as follows. For GLUE/MNLI we use $E = 3$, $\eta = 2e-5$, $\gamma = 0$. D-MFAC uses the default parameters from the original paper, e.g. $\eta = 1e-4$, $\lambda = 1e-6$, $\gamma = 0$ and we adopt the same values for S-MFAC for BERT-TINY/MINI. For BERT-BASE we use $\lambda = 5e-5$ for S-MFAC.

A.4 CIFAR-10/RN-20

For D/S-GGT we use window size $m = 100$, $k = 1\%$ and the grid in Table 4. We show the corresponding pairs (η, ϵ) for the best runs extracted from the search grids. In these experiments we use $E = 164$, $B = 128$ and decay the learning rate by a factor of $\gamma_\eta = 0.1$ at 50% and 75% of training. The final hyper-parameters for each method are summarized in table 5.

Table 4: Search grid for learning rate η and dampening ϵ for S/D-GGT.

η, ϵ	1e-7, 1e-6, 1e-5, 1e-4, 1e-3, 1e-2, 1e-1, 1
η_D, ϵ_D	loss: (1, 1e-6), accuracy: (1, 1e-5)
η_S, ϵ_S	loss: (1, 1e-6), accuracy: (1, 1e-5)

Table 5: Final hyper-parameters for CIFAR-10 / ResNet-20.

SGD	$\eta = 0.1, \mu = 0.9, \gamma = 5e-4$
D-GGT	$m = 100, \eta = 0.1, \epsilon = 1e-5, \gamma = 0$
S-GGT	$m = 100, \eta = 0.1, \epsilon = 1e-5, \gamma = 0$
D-MFAC	$m = 1024, \eta = 1e-3, \lambda = 1e-6, \mu = 0, \gamma = 1e-4$
S-MFAC	$k = 1\%, m = 1024, \eta = 1e-3, \lambda = 1e-4, \mu = 0, \gamma = 1e-4$
LR-MFAC	$\rho = 4, m = 1024, \eta = 1e-3, \lambda = 1e-6, \mu = 0, \gamma = 0$

Table 6: Hyper-parameters for SGD and S/D-MFAC for FFCV/ImageNet.

SGD	$\eta = 0.5, \mu = 0.9$
D-MFAC	$\eta = 1e-3, \lambda = 1e-6, \mu = 0$
S-MFAC	$\eta = 1e-3, \lambda = 1e-7, \mu = 0, k = 1\%$

B Memory savings.

In this section we detail the theoretical memory savings for the sparse preconditioners by computing the total memory in bytes and the ratio of dense over sparse preconditioners to describe de memory savings.

B.1 Sparse M-FAC vs Dense M-FAC

For M-FAC we will consider that $m = 1024$ and $k = d/100$.

Dense M-FAC stores a matrix $G \in \mathbb{R}^{m \times d}$ of 32 bit floats, having a total of $4md$ bytes, resulting in a theoretical memory footprint of $4096d$ bytes.

On the other hand, Sparse M-FAC stores multiple tensors:

- $\mathcal{I} \in \mathbb{R}^{m \times k}$ of 32 bit integers for the indices
- $\mathcal{V} \in \mathbb{R}^{m \times k}$ of 32 bit floats or 16 bit bfloat16s for the values
- $\xi \in \mathbb{R}^d$ of 32 bit floats for the error feedback
- $r_m \in \mathbb{R}^m$ of 32 bit floats to store the SP result
- $r_d \in \mathbb{R}^d$ of 32 bit floats to store the LCG result

When \mathcal{V} holds 16 bit bfloat16s, the memory footprint for $\mathcal{I}, \mathcal{V}, \xi, r_m, r_d$ altogether is $4mk + 2mk + 4d + 4m + 4d = 0.06md + 8d + 4m = 61.44d + 8d + 4m = 69.44d + 4m \approx 70d$.

When \mathcal{V} holds 32 bit floats, the memory footprint for $\mathcal{I}, \mathcal{V}, \xi, r_m, r_d$ altogether is $4mk + 4mk + 4d + 4m + 4d = 0.08md + 8d + 4m = 81.92d + 8d + 4m = 89.92d + 4m \approx 90d$.

In the end, the memory savings for M-FAC is $\frac{4096d}{90d} \approx 45.5 \times$ for float and $\frac{4096d}{70d} \approx 58.5 \times$ for bfloat16.

B.2 Sparse GGT vs Dense GGT

For GGT we will consider that $m = 100$ and $k = d/100$.

Dense GGT stores a matrix $G \in \mathbb{R}^{m \times d}$ of 32 bit floats, having a total of $4md$ bytes, resulting in a theoretical memory footprint of $400d$ bytes.

Sparse GGT stores the following tensors:

- $\mathcal{I} \in \mathbb{R}^{m \times k}$ of 32 bit integers for the indices
- $\mathcal{V} \in \mathbb{R}^{m \times k}$ of 32 bit floats for the values
- $\xi \in \mathbb{R}^d$ of 32 bit floats for the error feedback
- $r_m \in \mathbb{R}^m$ of 32 bit floats to store the SP result

The theoretical memory footprint for $\mathcal{I}, \mathcal{V}, \xi, r_m$ altogether is $4mk + 4mk + 4d + 4m = 8mk + 4d + 4m = 0.08md + 4d + 4m = 8d + 4d + 4m = 12d + 4m \approx 12d$. In the end, the memory savings for GGT is $\frac{400d}{12d} \approx 33.3 \times$.

C CUDA Kernels

In this section we describe our efficient CUDA kernels for large models in algorithmic form. We reiterate that M-FAC has two operations that have to be reimplemented when using a sparse ring buffer $G = (\mathcal{I}, \mathcal{V})$, the scalar products (SP) and linear combination of gradients (LCG). In the next paragraphs we provide a brief algorithmic description for SP and LCG.

C.1 SP Kernel

For this operation we have to compute the scalar product between each row in G and a general gradient g . The sparse matrix G is splitted into two matrices, the indices matrix $\mathcal{I} \in \mathbb{N}^{m \times k}$ and the values matrix $\mathcal{V} \in \mathbb{R}^{m \times k}$. We use 1024 thread blocks, each containing 1024 threads and one thread block will process one row. In the algorithm we will consider that \mathcal{I} and \mathcal{V} are 2-dimensional, but in practice they are 1-dimensional. We use $\omega \in \mathbb{R}^m$ to store result of the SP operation in Algorithm 2

Algorithm 2 SP kernel (CUDA)

```

1: Input:  $m, k, g, \mathcal{I}, \mathcal{V}, \omega$ 
2:  $mem$  is a shared memory buffer with  $T$  components
3:  $\sigma \leftarrow 0$  ▷ stores the partial dot product in current thread
4:  $Bid \leftarrow$  block id ▷ gives the row index in  $\mathcal{I}$  and  $\mathcal{V}$ 
5:  $Tid \leftarrow$  thread id
6:  $T \leftarrow$  number of threads in the block
7:  $r \leftarrow Bid$  ▷ row index
8: for  $j \in \{Tid < k, T\}$  do ▷  $j$  from  $Tid$  to  $k$  with step  $T$  (coalesced memory access)
9:    $i \leftarrow \mathcal{I}_{r,j}$ 
10:   $v \leftarrow \mathcal{V}_{r,j}$ 
11:   $\sigma \leftarrow \sigma + v \cdot g_i$  ▷ accumulate partial dot product
12: end for
13:  $mem_{Tid} \leftarrow \sigma$ 
14: parallel_reduce(mem, T) ▷ logarithmic sum: result is in  $mem_0$ 
15: if  $Tid = 0$  then
16:    $\omega_r \leftarrow mem_0$ 
17: end if

```

C.2 LCG Kernel

The LCG operation is more complex than the SP operation and requires providing more details. We will start from the compression operator from line 6 of Algorithm 1, which actually applies Top- k on the accumulator a_t , returning a compressed representation c_t (not to be confused with the vector c that stores the coefficients of the linear combination) - the c_t is placed on a specific row of $G = (\mathcal{I}, \mathcal{V})$ at each iteration t .

The Top- k operator is applied in blocks of size B_d (the subscript d means that this block is part of a d -dimensional vector), which is chosen automatically to be the maximum number of floating point values that can fit in the entire shared memory space for a thread block. For example, the A100 GPU from Nvidia has CUDA capability 8.0 and the maximum amount of shared memory per block is 163KB, meaning that we can store $B_d = 41728$ float32 values in the shared memory. The value k is inputted as a percentage at runtime and represents the density percentage of c_t . We convert this percentage to an actual density in each block B_d . For example, for $k = 1\%$ we will have around $B_k = B_d/100$ (we will further skip some implementation details).

The key detail of our LCG kernel is we use the shared memory of size B_d to accumulate partial linear combinations over slices of size (m, B_d) of the sparse matrix G and then write the result to the output $\omega \in \mathbb{R}^d$. This is possible because we apply Top- k operator in blocks of size B_d and we know the ends of the interval where we write the output to. Each thread block can process multiple slices of size (m, B_d) , depending on how large the model is. The pseudocode of the LCG kernel is provided in Algorithm 3.

D Sparse GGT.

In principle, the same sparsity format can be used for GGT as in the case of M-FAC. However, we would like to provide a slightly different approach just to show that an existing sparsity format is not completely efficient with respect to memory since they store redundant information. Our Sparse GGT uses the same sparsity format as S-MFAC and here we want to emphasize some drawbacks of COO format.

At a high level, we wish to leverage sparsity in the logical gradient history matrix $G \in \mathbb{R}^{m \times d}$. For this, we store it in the COOrdinate list sparse format, which requires storing matrix $\mathcal{V} \in \mathbb{R}^{m \times k}$ for values, matrix $\mathcal{R} \in \mathbb{Z}^{m \times k}$ for rows and $\mathcal{C} \in \mathbb{Z}^{m \times k}$ for columns. All these matrices can be stored in vector format, with dimension $m \cdot k$. This will be compatible with standard sparse operations, such as the Sparse Matrix-Matrix (SPMM) method in the PyTorch Sparse library [11].

Algorithm 3 LCG kernel (CUDA)

```

1: Input:  $B_d, B_k, d, m, k, c, \mathcal{I}, \mathcal{V}, \omega$ 
2:  $B \leftarrow$  total number of thread blocks
3:  $Bid \leftarrow$  block id ▷ gives the row index in  $\mathcal{I}$  and  $\mathcal{V}$ 
4:  $Tid \leftarrow$  thread id
5:  $T \leftarrow$  number of threads in the block
6:  $mem$  is a shared memory buffer with  $T$  components
7:  $mem \leftarrow 0$  ▷ initialize shared memory (the LCG accumulator) with zero
8: synchronize threads ▷ wait for all threads to finish initializing
9:  $n_{B_d} \leftarrow \lceil \frac{d}{B_d} \rceil$  ▷ how many blocks of size  $B_d$  we have
10:  $workload \leftarrow \lceil \frac{n_{B_d}}{B} \rceil$  ▷ how many blocks of size  $B_d$  each thread block processes
11: for  $i \in \{0 < workload\}$  do ▷ iterate through all slices  $(m, B_k)$  (workload) for the curret thread block
12:    $start_d \leftarrow B_d \cdot Bid \cdot workload + B_d \cdot i$  ▷ where slice starts in  $g$ 
13:    $end_d \leftarrow \min(d, start_d + B_d)$  ▷ where slice ends in  $g$ 
14:    $start_k \leftarrow B_k \cdot Bid \cdot workload + B_k \cdot i$  ▷ where slice starts in  $G$ 
15:    $end_k \leftarrow \min(B_k, start_k + B_k)$  ▷ where slice ends in  $G$ 
16:   for  $row \in \{0 < workload\}$  do ▷ iterate all rows in the slice  $(m, B_k)$  between  $(start_k, end_k)$ 
17:     for  $col \in \{start_k + Tid, \min(end_k, end_d), T\}$  do ▷ jump  $T$  steps (coalesced memory access)
18:        $i \leftarrow \mathcal{I}_{r,col}$  ▷ read index
19:        $v \leftarrow \mathcal{V}_{r,col}$  ▷ read value
20:        $mem_{i-start_d} += c_r \cdot v$  ▷ multiply the coefficient of current row with value
21:     end for ▷ finished processing one row
22:   synchronize threads
23: end for ▷ finished processing all rows
24: ▷ finished processing a slice of size  $(m, B_k)$ , now write result
25:   for  $i \in \{Tid < \min(B_d, d - start_d), T\}$  do ▷ write result (coalesced memory access)
26:      $\omega_{i+start_d} \leftarrow mem_i$  ▷ write result from  $mem$  to output  $\omega$ 
27:      $mem_i \leftarrow 0$  ▷ zerorize shared memory to prepare for the next step
28:   end for
29:   synchronize threads
30: end for

```

We will use the tuple $(\mathcal{R}, \mathcal{C}, \mathcal{V})$ to refer to the sparse buffer G . We distinguish between \mathcal{V} , which is the internal state of the sparse buffer (holding the k most significant values from a_t) and \mathcal{V}_t , which is the output of Top- k operator at a single step. *With slight abuse of notation, we call the compressed accumulator $c_t = (\mathcal{V}_t, \mathcal{I}_t)$ a sparse gradient, even though it is an accumulation of previous gradients.* The matrix \mathcal{C} is created in such a way that each row contains the index of that row (e.g. $[0, \dots, 0; 1, \dots, 1; \dots; m-1, \dots, m-1]$) and is represented as a single vector where the rows are concatenated (here is where we have redundancy, e.g. duplicated data - the values in this tensor never change).

Let $i \in \{0, \dots, m-1\}$ be an index indicating the location where the new gradient will be placed in the buffer $(\mathcal{R}, \mathcal{C}, \mathcal{V})$. At each step, we receive the accumulator a_t , the most significant k values \mathcal{V}_t and their corresponding indices \mathcal{I}_t . The expression $a_t[\mathcal{I}_t] \in \mathbb{R}^d$ will represent a “densified” version of a sparse vector, which contains zeros at indices $j \notin \mathcal{I}_t$ (sparse tensor which also contains the zeros - does not provide any memory reduction).

We integrate the values and indices in the internal buffers \mathcal{V} and \mathcal{I} in row i using the indices α and β . Since the sparse $G \in \mathbb{R}^{m \times k}$ and we have to compute the scalar product $\delta = G^T x$, we can easily transpose the sparse G by swapping the rows and columns in the SPMV call. The scalar products matrix $G^T G$ is updated by overwriting the i^{th} row and column by δ . At this point we can perform eigenvalue decomposition of $G^T G$ and finally compute the update direction u_t by preconditioning the sparse accumulator $a_t[\mathcal{I}_t]$. The full procedure is presented in Algorithm 4.

GGT results for CIFAR-10/ResNet-20. Our experimental setup covers ResNet-20 [15] ($d = 0.27M$) for CIFAR-10 [20]. We train models from scratch using SGD with momentum, dense and sparse GGT (99% sparsity) and M-FAC and low-rank M-FAC (rank 4). We decouple the weight decay γ from the gradient, and apply it in the optimizer, which allows us to compare the loss values. The results in Table 7 show validation accuracy on the ResNet20/CIFAR-10 experiment. We observe that 1) Dense(D) M-FAC reaches similar accuracy to SGD, whereas Dense(D) GGT achieves lower accuracy in this task; 2) Sparse(S) M-FAC reaches the same accuracy as the dense variant (and SGD); 3) Low-Rank(LR) M-FAC with rank 4 reaches $< 0.8\%$ lower accuracy relative to the best results.

Table 7: Results for ResNet-20 on CIFAR10. The first row reports the training loss and second row validation accuracy. The number in parentheses indicate stdev (for training loss, this is within 0.001).

	SGD	D-MFAC	S-MFAC	D-GGT	S-GGT	LR-MFAC
Loss	0.032	0.017	0.017	0.108	0.097	0.021
Acc.	92.16 (.10)	92.12 (.13)	92.25 (.21)	87.77 (.22)	87.73 (.34)	91.43 (.30)

Algorithm 4 Detailed Sparse GGT Implementation

```

1: Variables:  $\mathcal{V} \leftarrow 0 \in \mathbb{R}^{mk}$ ,  $\mathcal{R} \leftarrow 0 \in \mathbb{Z}^{mk}$ ,  $i \leftarrow 0$ ,  $G^T G \leftarrow 0 \in \mathbb{R}^{m \times m}$ 
2: Operators:  $\mathcal{C} \leftarrow \text{vec}([r \cdot 1_k]_{r=0}^{m-1}) \in \mathbb{Z}^{mk}$ 
3: procedure SPARSEGGT-STEP( $t, a_t \in \mathbb{R}^d, \mathcal{V}_t \in \mathbb{R}^k, \mathcal{I}_t \in \mathbb{Z}^k$ )
4:    $\alpha \leftarrow i \cdot k$ ,  $\beta \leftarrow \alpha + k$ ,  $\mathcal{V}_{\alpha:\beta} \leftarrow \mathcal{V}_t$ ,  $\mathcal{R}_{\alpha:\beta} \leftarrow \mathcal{I}_t$  ▷ integrate values and indices
5:    $\delta \leftarrow \text{SPMM}(\text{Sparse}(r = \mathcal{C}, c = \mathcal{R}, v = \mathcal{V}), \text{Dense}(a_t[\mathcal{I}_t]))$  ▷ compute  $G^T a_t[\mathcal{I}_t]$ 
6:    $\text{row}_i(G^T G) \leftarrow \delta$ ,  $\text{col}_i(G^T G) \leftarrow \delta$  ▷ update dot products in row and col  $i$ 
7:    $G^T G \leftarrow V \Sigma_m^2 V^T$ ,  $i \leftarrow (i + 1) \bmod m$  ▷ eigenvalue decomposition & index update
8:    $U_m \leftarrow \text{SPMM}(\text{Sparse}(r = \mathcal{R}, c = \mathcal{C}, v = \mathcal{V}), \text{Dense}(V \sqrt{\Sigma_m}^\dagger))$ 
9:    $u_t \leftarrow \frac{1}{\epsilon} (a_t[\mathcal{I}_t]) + U_m [(\Sigma_m + \epsilon I_m)^{-1} - \frac{1}{\epsilon} I_m] U_m^T (a_t[\mathcal{I}_t])$  ▷ compute GGT direction
10:  return  $u_t$ 
11: end procedure

```

E Compressing Preconditioners via Low-Rank Approximation and Error Feedback

In this section, we discuss an alternative approach for compressed preconditioners, via low-rank compression of the gradients. Specifically, we will implement the COMPRESS step in Algorithm 1 via a low-rank approximation of the gradient, using an efficient variant of power iteration [35]. Then, we consider the M-FAC algorithm, and reformulate its operations to leverage low-rank matrix operations for memory savings. We start by describing how the algorithm works a single layer, and then present the global algorithm, which computes preconditioning for the whole model.

Low-Rank M-FAC for a Single Layer. Assume that the gradient at a given layer of the model is represented by the s -dimensional tensor $g \in \mathbb{R}^{p_1 \times p_2 \times \dots \times p_s}$. To compress the tensor, we use a variant of power iteration [35] by firstly unfolding the tensor into a matrix $\tilde{g} \in \mathbb{R}^{p_1 \times p_{2:s}}$, where $p_{2:s} = \prod_{i=2}^s p_i$. This matrix is then iteratively multiplied by a rank ρ matrix $Q \in \mathbb{R}^{p_{2:s} \times \rho}$, which is reused from the previous iteration, to obtain the left decomposition matrix $P \in \mathbb{R}^{p_1 \times \rho}$. After orthogonalization of P , the updated right matrix Q is obtained from the relation $\tilde{g} = PQ^T$. Notice that P and Q have $(p_1 + p_{2:s})\rho$ elements which can be significantly smaller than $p_1 \cdot p_{2:s}$ for smaller ranks ρ . This compression procedure is outlined in Algorithm 5.

In order to “introduce” the current gradient g into the M-FAC preconditioner data structure, we firstly need to compute an inner product between previously stored gradients and g (see Equation 5).

In matrix representation the product between two gradients corresponds to the Frobenius inner product. Specifically, for a given low-rank representation of gradient matrices $\tilde{g}_i = P_i Q_i^T$ and $\tilde{g}_j = P_j Q_j^T$, the Frobenius product can be written as $\text{Tr}(\tilde{g}_i^T \tilde{g}_j) = \text{Tr}(Q_i P_i^T P_j Q_j^T) = \text{Tr}((P_j^T P_i)^T (Q_j^T Q_i))$. Notice that matrix products $P_j^T P_i$ and $Q_j^T Q_i$ are only of size ρ by ρ , so we compute them explicitly and then perform summation over their element-wise products to get the final result. As full gradients do not appear in this expression, we store just left and right gradients P_i and Q_i and update the M-FAC inner product matrix as needed.

The final preconditioned gradient update is computed as a weighted sum of previous gradients. The weights are computed via dynamic programming on top of the inner product values as in the original M-FAC. The final weighted sum of gradients is obtained by sequentially adding gradients reconstructed from their low-rank representation $g_i = P_j Q_j^T$.

Global Low-Rank M-FAC. To obtain an equivalent algorithm to the original M-FAC, independent per-layer steps are not sufficient as we would lose cross-layer correlation information. Instead, we use linearity of the inner product to compute the final result efficiently. In the original version of M-FAC, a current complete gradient from a L -layered model is represented as a concatenation of flattened per-layer gradients $\hat{g} = (\hat{g}^1 \ \hat{g}^2 \ \dots \ \hat{g}^L)^T$, where \hat{g}^i is the gradient from layer i . In this, representation an inner product between two gradients \hat{g}_i and \hat{g}_j can be expressed in a block form as $(\hat{g}_i, \hat{g}_j) = \sum_{\ell=1}^L (\hat{g}_i^\ell, \hat{g}_j^\ell)$. This dot product is then used to update the inner product matrix $G^T G$.

Algorithm 5 Power iteration compression algorithm [35]

```

1: procedure POWERCOMPRESS(gradient tensor g, previous Q) ▷ applied for each layer
2:    $\tilde{g} \leftarrow g.\text{RESHAPE}(p_1, p_{2:s})$ 
3:    $P \leftarrow \tilde{g}Q$ 
4:    $P \leftarrow \text{ORTHOGONALIZE}(P)$ 
5:    $Q \leftarrow \tilde{g}^T P$ 
6:   return ( $P, Q$ )
7: end procedure

```

Algorithm 6 Low Rank M-FAC preconditioning

```

1: INPUT: per-layer compressed  $((P^1, Q^1), \dots, (P^L, Q^L))$  gradients
2: STATE: per-layer ring buffers  $G^\ell$  with compressed gradient history; full inner products  $G^T G$ 
3: procedure LOW RANK M-FAC( $(P^1, Q^1), \dots, (P^L, Q^L)$ )
4:    $\delta \leftarrow$  zero vector of size  $m$  ▷ new full inner product
5:   for each layer  $\ell \in \{1, 2, \dots, L\}$  do ▷ aggregate inner products across the whole model
6:     Update  $G^\ell$  with current gradient  $(P^\ell, Q^\ell)$ 
7:     for each time step  $\tau \in \{t - m + 1, \dots, t\}$  do
8:        $\delta_{t-\tau} \leftarrow$  low-rank inner product  $\text{Tr}((g_\tau^\ell)^T (P^\ell (Q^\ell)^T))$ 
9:     end for
10:  end for
11:  Update row and column in  $G^T G$  from  $\delta$ 
12:  M-FAC: compute summation weights  $w \in \mathbb{R}^m$  from  $G^T G$ 
13:  for each layer  $\ell \in \{1, 2, \dots, L\}$  do
14:     $u_t^\ell \leftarrow \epsilon^{-1} P^\ell (Q^\ell)^T + \sum_{\tau=t-m+1}^t w_\tau g_\tau$  ▷ aggregate gradients from the ring buffer
15:  end for
16:  return vector of per-layer updates  $u_t$ 
17: end procedure

```

In the context of our efficient scheme for single-layer low-rank update, we replace each inner product block by its low-rank counterpart to obtain the equivalent values. Recall that the computation of summation weights in the M-FAC needs access only to these inner products, so this part of the algorithm remains the same. The final gradient update is computed per-layer and we rely on linearity of the sum again to share the summation weights and dampening coefficient ϵ between layers. For more details refer to the pseudocode in Algorithm 6.

Results for Low-Rank M-FAC. We present and discuss the experiments for Low-Rank M-FAC on CIFAR-10/ResNet-20 in Table 7 and hyper-parameters in Appendix A. Next, we present an ablation study of low rank decomposition on both CIFAR-10/ResNet-20 and GLUE/MNLI for BERT-TINY.

To determine how the size of the decomposition rank ρ affects the effectiveness of the low rank M-FAC algorithm, we perform a series of experiments on ResNet-20 and BERT models. For ResNet-20 we use CIFAR-10 dataset and the same parameters as in the main experiments. For BERT family we use TINY, MINI and BASE variants and evaluate them on MNLI task from GLUE benchmark. For both setups we vary the rank from 1 to 8 and report the final test accuracy in the Table 8.

We observe that the decomposition rank significantly affects smaller BERT models but barely influences BERT-BASE and RN-20 model results. While the exact reason for such behaviour is not obvious, we hypothesise that for RN-20 the decomposition is effective even at rank 1 due to gradient tensors already having a small first dimension, resulting in small compression error. We also note that Rank 8 BERT-BASE run diverged, requiring more investigation into the stability of the training.

Table 8: Test accuracy on CIFAR-10 dataset for ResNet-20 (RN-20) and on MNLI for BERT-TINY, -MINI and -BASE, trained with Low-Rank M-FAC with different decomposition ranks ρ .

rank ρ	RN-20	TINY	MINI	BASE
1	91.40	57.34	66.88	84.42
2	91.19	63.49	68.76	84.44
4	91.43	66.44	70.93	84.45
8	91.13	67.90	72.22	—